

MET alterations are enriched in lung adenocarcinoma brain metastases, defining a distinct biologic subtype

Timothy F. Burns,^{1,2,3} Sanja Dacic,⁴ Anish Chakka,⁵ Ethan Miller,¹ Maria A. Velez,¹ Ashwin Somasundaram,¹ Saveri Bhattacharya,¹ Autumn Gaither-Davis,¹ Princey Devadassan,¹ Jingxiao Jin,¹ Vinod Kumar,¹ Arjun Pennathur,⁶ Joanne Xiu,⁷ Matthew Oberley,⁷ Michael J. Glantz,⁸ Sonikpreet Aulakh,⁹ Uma R. Chandran,⁵ Riyue Bao,^{1,3} Curtis Tatsuoka,^{10,3} and Laura P. Stabile^{2,3}

¹Division of Hematology/Oncology, Department of Medicine, and ²Department of Pharmacology and Chemical Biology, University of Pittsburgh School of Medicine, Pittsburgh, Pennsylvania, USA. ³UPMC Hillman Cancer Center, Pittsburgh, Pennsylvania, USA. ⁴Department of Pathology, ⁵Department of Bioinformatics, and ⁶Department of Cardiothoracic Surgery, University of Pittsburgh School of Medicine, Pittsburgh, Pennsylvania, USA. ⁷Caris Life Sciences, Phoenix, Arizona, USA. ⁸Department of Neurosurgery, Penn State Health Milton S. Hershey Medical Center, Hershey, Pennsylvania, USA. ⁹Department of Medical Oncology, West Virginia University, Morgantown, West Virginia, USA. ¹⁰Department of Biostatistics, University of Pittsburgh School of Medicine, Pittsburgh, Pennsylvania, USA.

Non-small cell lung cancer exhibits the highest rates of brain metastases (BMs) among all solid tumors, presenting a major clinical challenge. The development of novel therapeutic strategies targeting BMs is clearly needed. We identified a significant enrichment of *MET* amplification in lung adenocarcinoma (LUAD) BMs compared with primary LUAD and extracranial metastases in oncogene driver-negative patients. Of note, *MET*-amplified BMs were responsive to *MET* inhibitors *in vivo*, including models with acquired *MET* amplification at the time of metastasis. *MET* alterations (amplifications and/or mutations) were also more frequently detected in circulating tumor DNA from patients with LUAD BMs than in those without BMs. *MET*-altered BMs also demonstrated unique genomic features compared with non-*MET*-altered BMs. Transcriptomic analyses revealed that in contrast to *MET* WT BMs, *MET*-amplified BMs exhibited a more inflamed tumor microenvironment and displayed evidence of metabolic adaptation, particularly a reliance on glycolysis in contrast to OXPHOS in *MET* WT BMs. Furthermore, *MET*-amplified BMs demonstrated evidence of epithelial-mesenchymal transition signaling, including increased expression of TWIST1. Patients with *MET*-amplified BMs had significantly shorter overall survival. These findings highlight *MET* amplification as a critical driver of LUAD BMs, emphasizing its potential as a therapeutic target.

Introduction

Lung cancer remains the leading cause of cancer-related deaths in the United States (1). Among solid tumors, non-small cell lung cancer (NSCLC) has the highest incidence of brain metastases (BMs) (2–4). Approximately 25% of patients with NSCLC present with BMs at diagnosis, and more than 40–50% eventually develop BMs during their disease course (4, 5). BMs are more common in patients with lung adenocarcinoma (LUAD) histology (5, 6), and the prognosis of patients with BMs and LUAD histology is improved compared with those with non-LUAD histologies; however, the prognosis for patients with BMs without a CNS-targetable oncogenic driver (*EGFR* mutation or *ALK*, *RET*, or *ROS1* translo-

cation) remains poor (6–8). Advances in classifying NSCLC into molecularly defined subgroups responsive to specific therapies have shifted the treatment paradigm from standard chemotherapy to personalized targeted therapies and immunotherapy. Unfortunately, despite these advances, the brain often remains the primary site of disease progression, even in patients for whom the systemic disease is controlled by targeted therapies or immunotherapy (9–11). This underscores the urgent need for more effective treatment strategies to improve outcomes in this challenging patient population.

The HGF/*MET* pathway has emerged as a promising target for treatment and/or prevention of NSCLC BMs. Studies have shown increased total and phosphorylated *MET* expression in NSCLC BMs and high HGF levels in astrocytes (12–15). *MET* is a receptor tyrosine kinase that binds to HGF, activating signaling pathways that drive cell proliferation, epithelial-mesenchymal transition (EMT), motility, invasion, angiogenesis, and metastasis (16). In NSCLC, *MET* pathway dysregulation occurs through *MET* or HGF protein overexpression, *MET* amplification, or *MET* mutations (17, 18). *MET* amplification is detected in 2–4% of primary NSCLC tumors (19, 20) and is associated with poor prognosis (21, 22). It is also a well-established mechanism of acquired resistance to *EGFR* tyrosine kinase inhibitors (TKIs) (23, 24). Additionally, *MET* exon 14 skipping mutations (*METΔex14*) have been identified in 2–4% of NSCLC cases (20, 21, 25–28). Both *MET* amplification and *METΔex14* mutations are clinically actionable alterations in NSCLC, as dramatic responses to *MET* TKIs have been observed

Conflict of interest: TFB reports over the last 2 years receiving compensation from the following as a Data Safety and Monitoring Board member: Advarra Inc. (Lantern Pharma); participation on scientific advisory boards for Janssen Scientific Affairs LLC, AstraZeneca, Eli Lilly Inc., Genentech, Caris Life Sciences, Adcendo Aps, and Bristol Myers Squibb; consulting fees from Pfizer; and institutional research funds from Novartis (all to institution). SD is a consultant for AstraZeneca and participates on advisory boards for AstraZeneca and Genentech Roche. SA has received consulting fees from Caris Life Sciences for ad hoc review of molecular profiling cases and participation in Caris's molecular tumor board, as well as one-time consulting fees from Servier, SpringWorks Therapeutics Inc., PER, and Novocure.

Copyright: © 2025, Burns et al. This is an open access article published under the terms of the Creative Commons Attribution 4.0 International License.

Submitted: May 9, 2025; **Accepted:** December 16, 2025; **Published:** December 18, 2025.

Reference information: *J Clin Invest*. 2026;136(4):e194708.

<https://doi.org/10.1172/JCI194708>.

in patients with these alterations (27–35). In the GEOMETRY mono-1 study, the MET TKI capmatinib showed efficacy in extracranial lesions with a *MET* gene copy number (GCN) ≥ 10 (31). However, MET TKIs have shown overall response rates exceeding 50% with a lower cutoff (MET/CEP7 ratio ≥ 4) when assessed by FISH (32–34) or circulating tumor DNA (ctDNA) analysis (35, 36). Furthermore, MET TKI activity has been reported at an even lower cutoff (MET/CEP7 ratio ≥ 2) in the setting of *EGFR* mutant NSCLC with *MET* amplification (24). Despite these findings, the level of *MET* amplification required for MET dependency in BMs remains unclear. The MET TKIs capmatinib and tepotinib have shown preliminary evidence of activity against *MET**Alex14* mutant BMs, as well as in *MET*-amplified primary NSCLC (31, 35, 37, 38). Additionally, tepotinib has demonstrated efficacy in inhibiting *MET*-amplified BM growth in orthotopic preclinical models (39), and savolitinib has demonstrated activity against *MET*-amplified BMs (40). Interestingly, 2 case reports of patients with NSCLC BMs, one with a rare *MET* gene fusion found in the primary lung lesion (41) and the other with concurrent *ALK* fusion and *MET* amplification found in the BM (42), both demonstrated rapid intracranial responses to MET TKIs. It should be noted that in the second report, it is unclear whether *MET* amplification or the *ALK* fusion was the driver oncogene since both alterations are known to be sensitive to crizotinib.

Defining the molecular genotype of BMs is crucial to identifying potential therapeutic targets in patients with NSCLC BMs. However, molecular studies in BMs are limited compared with the numerous studies that have defined the molecular landscape of primary NSCLC tumors. A landmark study comparing paired primary and BMs from lung, melanoma, and breast cancers revealed that distinct targetable alterations (PI3K/AKT/mTOR, CDK, and HER2/EGFR) are enriched in BMs compared with primary lesions (43). Notably, 53% of BMs harbored clinically targetable alterations that were not detected in the paired primary tumors, though this study included only 38 lung cancer BM cases. Interestingly, in this small cohort, *MET* amplification was found in 4/34 (11.8%) of nonsquamous NSCLC BMs, with half of these cases exhibiting BM-specific *MET* amplification not detected in the primary tumor. A separate study of 73 LUAD BMs found higher amplification frequencies of *MYC*, *YAPI*, and *MMP13* compared with primary LUAD tumors in The Cancer Genome Atlas dataset (44). More recent genomic studies of NSCLC BMs have reported higher frequencies of distinct alterations, including *TP53*, *KRAS*, and *CDKN2A* mutations, in BMs compared with extracranial sites (45, 46). While one study did not assess gene amplifications (46), our previous study (45) identified a 2-fold increase in *MET* amplification in NSCLC BMs compared with primary NSCLC (4.4% vs. 2.4%). These studies utilized next-generation sequencing–based (NGS-based) platforms and GCN to determine amplification, which is less sensitive than FISH for detecting amplification, as NGS requires higher GCN cutoffs to call focal amplification and exclude aneuploidy. To date, no previous BM studies have specifically evaluated *MET* amplification using FISH.

In this study, we identified a significant enrichment in the frequency of *MET* amplification in LUAD BMs compared with both primary LUAD and liver metastases. Remarkably, these *MET* amplification events occurred in patients lacking oncogenic drivers who

had not received prior targeted therapy and were not simply due to an acquired *MET* amplification at the time of resistance. Our findings reveal a distinct molecular and transcriptomic landscape of LUAD BMs, characterized by immune and metabolic adaptations as well as induction of EMT that differentiate primary LUAD from LUAD BMs, as well as *MET*-altered (amplified and/or mutated) BMs from non-*MET*-altered BMs. Furthermore, we found that patients with lung cancer with *MET*-amplified BMs have significantly worse overall survival (OS) compared with those without *MET* amplification, emphasizing the aggressive nature of these tumors. Importantly, our data suggest that a liquid biopsy approach may serve as a viable approach for detecting BM-specific *MET* alterations as these were more frequently detected in ctDNA from patients with LUAD BMs than in those without BMs. Effective treatments for patients with lung cancer BMs represent an unmet need in current oncology clinical care. Results from this study provide critical insights into the biology of MET-driven LUAD BMs and suggest that targeting *MET* amplification, along with the associated immune and metabolic pathways, could offer therapeutic opportunities for patients with LUAD BMs who lack targetable extracranial oncogenic drivers.

Results

Acquired MET amplification in a LUAD BM that was responsive to capmatinib. A patient seen in our clinics with locally advanced (stage IIIA, T3N2M0; AJCC Cancer Staging Manual, seventh edition) LUAD underwent biopsy of the primary LUAD and lymph nodes prior to treatment; no molecular testing was performed at that time. FISH for *ALK*, *MET*, *RET*, and *ROS1* were all negative for amplification or gene arrangement. The patient subsequently underwent 3 cycles of neoadjuvant cisplatin/docetaxel prior to surgery. As the patient had microscopic N2 disease after surgery, they underwent postoperative radiation followed by observation. Unfortunately, after 5 months of observation, the patient developed a BM (Figure 1A). Genotyping of the resected BM using NGS was negative for *EGFR*, *KRAS*, *BRAF*, and *PIK3CA* mutations. Programmed cell death ligand 1 (PD-L1) immunostaining was also negative. Although the primary LUAD from this patient was negative for *MET* FISH (MET/CEP7 ratio = 0.98), FISH analysis of the BM revealed *MET* amplification with a MET/CEP7 ratio of 11.7. A patient-derived xenograft (PDX) model from the brain biopsy (PDX 16-16) was generated (47), and in vivo treatment with the MET TKI capmatinib (5 mg/kg body weight) significantly reduced tumor growth by 68.4% compared with vehicle control (Figure 1B). Of note, we have previously published that the BM PDX 16-16 expressed high levels of pMET (47), and in Supplemental Figure 1 (supplemental material available online with this article; <https://doi.org/10.1172/JCI194708DS1>), we have demonstrated that tumors from this experiment had high levels of total MET and pMET expression and that pMET is significantly inhibited after capmatinib treatment. This case report highlights the discordance between the molecular profiles of primary LUAD and its corresponding BM and the potential of *MET* amplification as a therapeutic target in BMs.

To assess the therapeutic effects of MET inhibition in the context of brain metastasis, we utilized an intracardiac injection metastasis model using *MET*-amplified H1993 LUAD cells. Of note, this cell line acquired a *MET* amplification during metastasis to the lymph node as the cell line derived from the primary tumor (H2073)

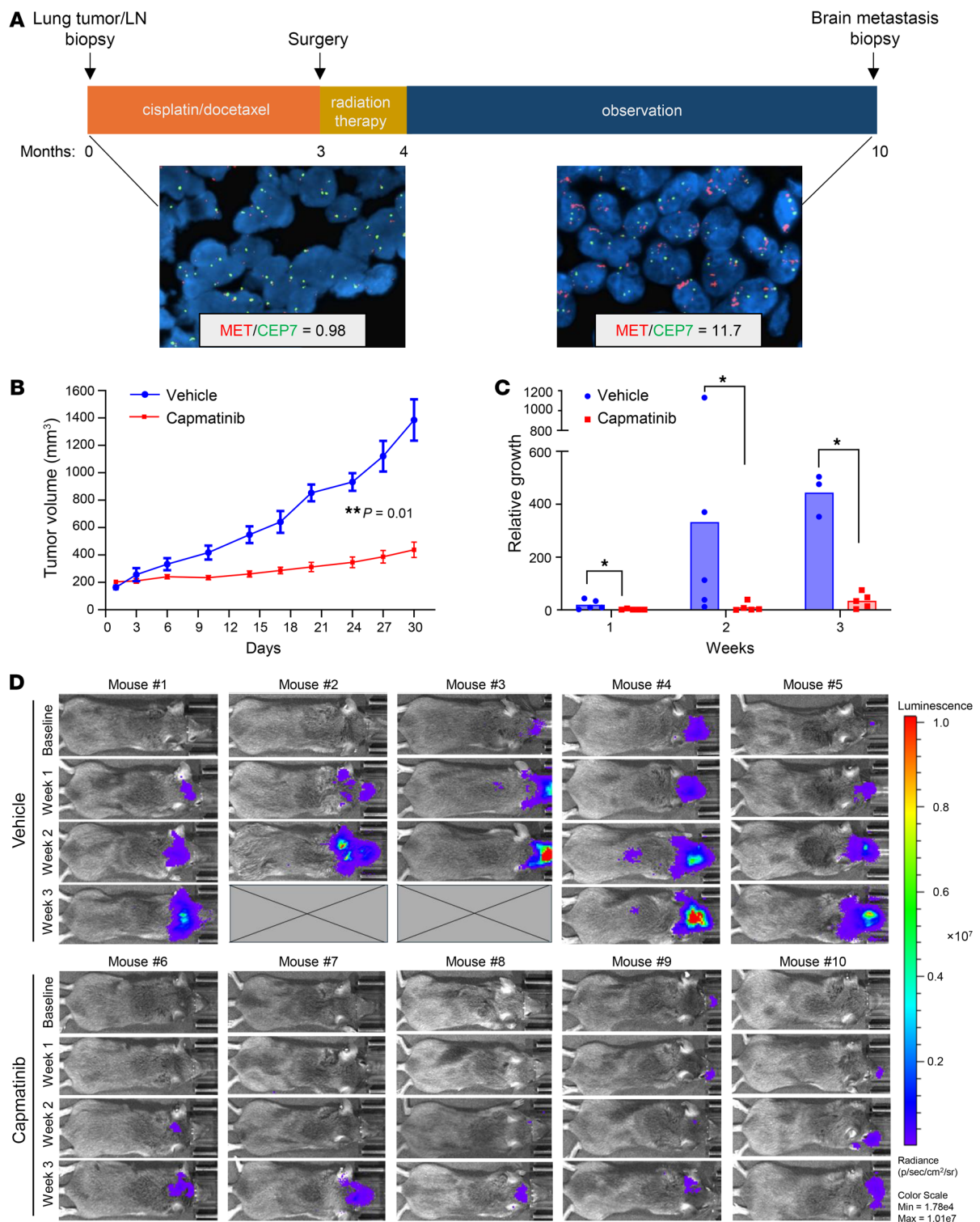


Figure 1. Acquired *MET* amplification in a LUAD BM that was responsive to capmatinib. (A) Timeline summarizing the treatment course, tumor biopsies, and *MET* amplification status. *MET* FISH images (×40 original magnification) are shown for the primary tumor biopsy at the time of diagnosis and 10 months later at the time of metastatic brain tumor biopsy. Red signals, *MET*; green signals, centromere 7 (CEP7). (B) A PDX model was established from patient 16-16 BM resection specimen. Mice were randomized to receive vehicle (0.25% w/v methyl cellulose) or capmatinib (5 mg/kg) by oral gavage 5 times per week for 4 weeks. Results are presented as mean tumor volume ± SEM of 6 tumors/group. Data were assessed by 2-tailed Student’s *t* test; ***P* = 0.01. (C) Luciferase-labeled H1993 LUAD cells were injected intracardially into SCID mice and monitored for metastatic spread. Mice were randomized to receive either vehicle (0.25% w/v methyl cellulose) or capmatinib (5 mg/kg) via oral gavage, administered 5 times per week for 3 weeks. Bioluminescent signal intensity in the head region was quantified relative to baseline and is presented as the mean ± SD. Statistical analysis was performed using the Mann-Whitney test; **P* < 0.05. (D) Longitudinal bioluminescent imaging of individual mice over the course of treatment. All images were acquired and analyzed using Living Image Software (Perkin Elmer) and set to the same intensity scale for comparison. “X” represents mice that died prior to the end of the 3-week treatment period.

Table 1. Selected patient characteristics for UPMC *MET* FISH cohort

	Primary LUAD, N = 459	BMs, N = 171	Liver metastases, N = 76	P value ^a
Age at diagnosis in yrs, mean (± SD) range	68.2 (± 10.6) 33–92	61.1 (± 9.4) 37–83	66.0 (± 10.9) 33–92	NS
Sex, N (%)				
Male	218 (47.5)	85 (49.7)	33 (43.4)	NS
Female	241 (52.5)	86 (50.3)	43 (56.6)	
Race, N (%)				
White	412 (89.8)	156 (91.2)	67 (88.2)	NS
Black/African American	34 (7.4)	13 (7.6)	8 (10.5)	
American Indian/Alaska Native	1 (0.2)	0	0	
Asian	5 (1.1)	1 (0.6)	1 (1.3)	
Other ^b	1 (0.2)	0	0	
Unknown ^c	6 (1.3)	1 (0.6)	0	
Smoking status, N (%)				
Ever	391 (85.2)	162 (94.7)	61 (80.3)	0.01
Never	68 (14.8)	9 (5.3)	15 (19.7)	
Stage, N (%)				
I–II	207 (45.1)	0	0	NA
III	76	0	0	
IV	169 (36.8)	171 (100)	76 (100)	
Unknown	7 (1.5)	0	0	NA
Metastases N (%)				
Brain				
Synchronous	53 (11.6)	114 (66.7)	10 (13.2)	NA
Metachronous	46 (10.0)	57 (33.3)	12 (15.8)	
None	358 (78.0)	0	51 (67.1)	
Unknown	2 (0.4)	0	3 (3.9)	
Liver				
Synchronous	18 (3.9)	9 (5.3)	51 (67.1)	NA
Metachronous	41 (9.0)	16 (9.3)	25 (32.9)	
None	398 (86.7)	145 (84.8)	0	
Unknown	2 (0.4)	1 (0.6)	0	
Alive at last follow-up, N (%)	174 (37.9)	12 (7.0)	7 (9.2)	<0.0001

^a χ^2 test was used to determine P values. ^bA patient who chose not to define their race and alternatively selected "other" instead of one of the other available categories. ^cNo data available.

in the same patient lacked a *MET* amplification (48). Following injection, metastatic progression was monitored weekly using in vivo bioluminescence imaging, with treatment initiated upon detection of a predefined signal intensity in the head region, typically the first site of metastasis of this cell line. Imaging was performed weekly for 3 weeks. Ex vivo imaging confirmed BM presence in all mice included in the study. Across all time points, signal intensity in the head region was significantly higher in the vehicle-treated mice compared with those receiving capmatinib (Figure 1, C and D). Notably, 2 mice from the control group succumbed to BM-related complications prior to the final imaging time point. This finding demonstrates that *MET* inhibition significantly suppresses BM outgrowth of *MET*-amplified LUAD cells.

MET amplification is more frequently observed in LUAD BMs compared with extracranial metastases and primary LUAD. To understand if this molecular divergence observed between primary LUAD and BMs was a frequent event, we evaluated a large cohort of patients to assess the frequency and clinical impact of *MET* amplification in metastatic sites. Previous studies assessing *MET* amplification

in lung cancer BMs primarily used NGS-based platforms, which are less reliable than FISH and require higher GCN cutoffs to detect amplification and exclude aneuploidy. We therefore evaluated 459 primary LUAD, 171 LUAD BMs, and 76 liver metastases for *MET* amplification using FISH (*MET*/*CEP7* ratio ≥ 2) (Table 1). We demonstrated that *MET* amplification was significantly enriched in LUAD BMs (16.4%) compared with primary LUAD (3.7%; $P < 0.0001$) or liver metastases (5.3%; $P = 0.022$), suggesting *MET* amplification may be a frequent and potentially targetable alteration in LUAD BMs (Figure 2A). We performed *MET* IHC in 49/171 (29%) BMs, including 36 non-*MET*-amplified and 11 *MET*-amplified BM cases. Of note, this subset of patients appears to be representative of the larger cohort in terms of patient characteristics (Supplemental Table 1). We observed a statistically significant increase in *MET* expression in the *MET*-amplified group, as assessed by both staining intensity and H-score ($P < 0.0001$) (Figure 2B). We found that high *MET* amplification (*MET*/*CEP7* ratio ≥ 4) was present in 6.5% of BMs versus 1.3% of primary LUADs. In addition, in a subset of 31 paired primary LUAD and BM samples, *MET* amplification was present in

3/31 (10%) BMs, while none of the matched primary tumors were amplified. Remarkably, the presence of a targetable oncogenic driver was an infrequent event in these patients, and there were no cases in which a prior targeted therapy had been received. Among the 5 BM cases with an *EGFR* mutation and 1 with *ALK* rearrangement, none had a *MET* amplification, while 1 *EGFR* mutant case had a *MET* non-exon 14 skipping mutation. The demographics and clinical characteristics of the BM cohort, stratified by *MET* amplification status, are summarized in Table 2. Patients with *MET*-amplified BMs were more likely to be female, and the overwhelming majority of these patients were current/former smokers compared with those with non-*MET*-amplified BMs. There was no significant difference in the timing (synchronous vs. metachronous) of BMs between patients with and without *MET* amplification. We validated these findings using an NGS dataset from Caris Life Sciences with over 30,000 patients, demonstrating that *MET* amplification is 5 times more frequent in BMs compared with primary LUAD ($P < 0.0001$) and 2.2 times more frequent than in extracranial sites (non-BMs) ($P < 0.0001$; *MET* copy number ≥ 6) (Figure 2C).

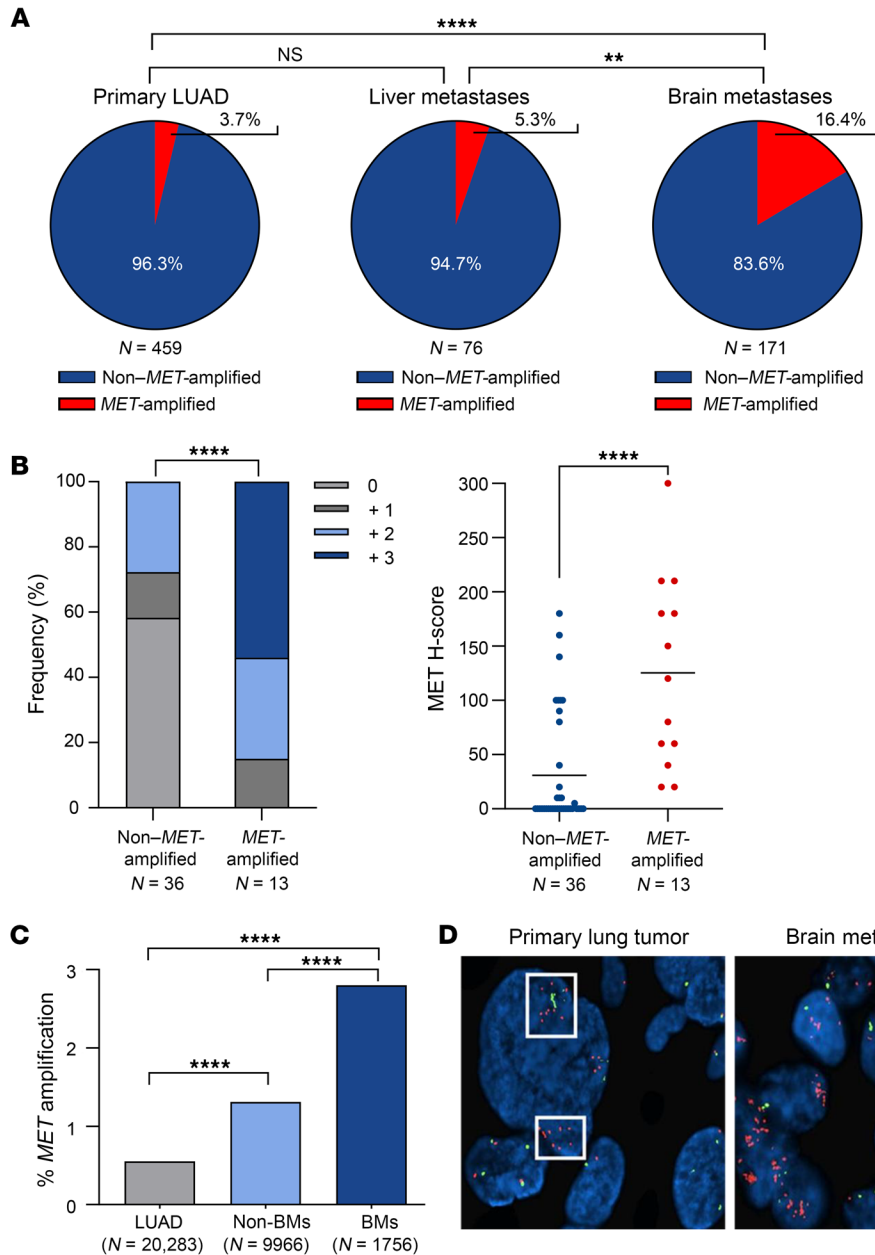


Figure 2. MET amplification is more frequently observed in LUAD BMs compared with extracranial metastases and primary LUAD. (A) Pie charts showing the frequency of MET amplification by FISH (MET/CEP7 ratio ≥ 2.0) in primary LUAD, liver metastases, and BMs in the UPMC cohort. Fisher's exact test, 2-sided; ** $P < 0.01$ ($P = 0.002$ exact), **** $P < 0.00001$. (B) MET protein expression by frequency of IHC staining intensity (0, +1, +2, +3; χ^2 test; **** $P < 0.0001$) and MET H-score (Student's *t* test, 2-tailed; **** $P < 0.0001$) in non-MET-amplified and MET-amplified BMs. Horizontal lines represent mean values. (C) Frequency of MET amplification by NGS copy number alteration (cutoff ≥ 6) in primary NSCLC, non-BMs, and BMs in the Caris cohort. χ^2 test; **** $P < 0.0001$. (D) Representative MET FISH images (captured at $\times 40$ original magnification and enlarged) from a matched primary LUAD and BM from the same patient. White boxes represent areas of focal MET amplification. Red signals, MET; green signals, CEP7.

We then asked if MET amplification was a rare preexisting event in the primary tumor that was subsequently enriched in the resulting BMs or whether it was truly a de novo event. Interestingly, we found examples in our matched primary LUAD and BM sets where rare cells from the primary lung tumor had focal clusters of amplified cells (Figure 2D). Rare MET-amplified clones likely preexist in the primary tumor, as focal MET amplification was observed in primary LUADs of patients with MET-amplified BMs (Figure 2D, white boxes). Since we found evidence of focal MET amplification in the primary tumor, we sought to determine whether this finding predicted the development of BMs. To assess this, we identified a cohort of NSCLC patients with and without focal MET amplification in the primary lung tumor (Supplemental Table 2). A retrospective chart review was conducted to determine the timing of metastasis and if patients developed BMs. BMs were confirmed based on imaging findings suggestive of BMs on a CT or MRI scan

of the brain, a radiology report indicating BMs, or a brain biopsy confirming metastatic spread to the brain. Among the 85 patients with focal MET amplification, 28 (33%) developed BMs, compared with 49 (37%) of the 131 patients without focal MET amplification in our cohort. There was no statistically significant difference in the frequency of BMs between the 2 groups ($P = 0.5$). When evaluating the timing of metastatic spread, 29 patients (59%) in the non-MET-amplified group had synchronous metastases (occurred within 2 months of diagnosis), while 20 (41%) had metachronous metastases (occurred after 2 months of diagnosis). Among the patients with focal MET amplification, 17 (61%) had synchronous metastases and 11 (39%) had metachronous metastases. There was no significant difference in the timing of BMs between the 2 groups ($P = 0.9$). These results show that focal MET amplification was not a predictor of BMs nor did it influence the timing of the development of BMs in patients with NSCLC.

Table 2. Selected patient characteristics for MET FISH BM cohort

	Non-MET-amplified BMs, N = 143	MET-amplified BMs, N = 28	P value ^A
Age at diagnosis in yrs, mean (± SD) range	60.7 (± 9.4) 37–83	63.1 (± 9.4) 47–80	NS
Sex, N (%)			
Male	73 (51.0)	12 (42.9)	NS
Female	70 (49.0)	16 (57.1)	
Race, N (%)			
White	130 (90.9)	26 (92.9)	NS
Black/African American	11 (7.7)	2 (7.1)	
American Indian/Alaska Native	0	0	
Asian	1 (0.7)	0	
Other ^B	0	0	
Unknown ^C	1 (0.7)	0	
Smoking status, N (%)			
Ever	95 (66.4)	27 (96.4)	0.0005
Never	48 (33.6)	1 (3.6)	
Metastases ^D , N (%)			
Brain			
Synchronous	94 (65.7)	20 (71.4)	NS
Metachronous	49 (34.3)	8 (28.6)	
Liver			
Synchronous	7 (4.9)	2 (7.15)	NS
Metachronous	14 (9.8)	2 (7.15)	
None	121 (84.6)	24 (85.7)	
Unknown	1 (0.7)	0	
Alive at last follow-up, N (%)	11 (7.7)	1 (3.6)	NS

^A χ^2 test was used to determine P values. ^BA patient who chose not to define their race and alternatively selected “other” instead of one of the other available categories. ^CNo data available.

^DSynchronous metastases occurred within 2 months of diagnosis; metachronous metastases occurred after this 2-month period.

MET alterations detected in ctDNA are found more often in patients with BMs. There is an unmet clinical need for noninvasive methods to detect *MET* alterations to identify patients with BMs who will benefit from *MET* TKIs. Although the ability of blood-based ctDNA assays to detect alterations present in BMs is diminished (49–51), we hypothesized that *MET* alterations would be more common in patients with BMs that had undergone ctDNA testing. We therefore examined a cohort of patients with metastatic NSCLC ($N = 277$) who underwent standard-of-care ctDNA testing at our institution with the Guardant360 platform to evaluate the presence of *MET* alterations in association with BMs. We observed that *MET* alterations detected by ctDNA were significantly more frequent in patients with BMs (15.6%) compared with patients without (7%) ($P = 0.023$) (Figure 3A). This appears to be driven primarily by the increased frequency of *MET* amplifications detected in patients with BMs (6.7%) compared with those without BMs (1.6%) ($P = 0.035$) (Figure 3B). While *MET* mutations were also more frequent in patients with BMs (8.9%) compared with those without BMs (5.3%), this difference was not statistically significant (Figure 3C). These findings suggest a potential role of ctDNA as a noninvasive method for detecting *MET* alterations, particularly amplifications, which may identify patients with BMs who are more likely to respond to *MET* TKIs.

LUAD BMs have a distinct mutational profile compared with primary LUAD tumors. We next performed targeted NGS to compare other alterations, including *MET* mutations, in 180 primary LUAD cases and 74 LUAD BM cases (Table 3). We found that mutations in *TP53*, *KRAS*, *SMAD4*, *APC*, *MET*, *RBI*, *STK11*, *RET*, *FGFR3*, *VHL*, *ALK*, *ABL1*, and *FLT3* were significantly more prevalent in LUAD BMs compared with primary LUAD (Figure 4). Interestingly, several of these alterations that were rare (*TP53*, *KRAS*, *MET*, *STK11*, *RET*, *FGFR3*, *VHL*, *ALK*, *ABL1*, and *FLT3*; 0–6%) or entirely absent (*SMAD4*, *APC*, and *RBI*) in primary LUAD samples were frequently observed (>20%) in LUAD BM samples. Complete lists of variants found in primary LUAD and LUAD BM cases are provided in Supplemental Tables 3 and 4, respectively. In addition, these differences were driven by specific variants that differ between these groups (Supplemental Figure 2A and Supplemental Figure 3). For example, 2 DNA-binding domain mutations in *TP53*^{R158L} and *TP53*^{V157F} were significantly increased in LUAD BMs compared with primary LUAD (Supplemental Figure 3A). Remarkably, the relatively rare *KRAS*^{Q61X} point mutations were significantly enriched in LUAD BMs compared with primary LUAD (Supplemental Figure 3D). Of note, the frequency of *MET* mutations was significantly increased in LUAD BMs (22%) compared with primary LUAD (12%) ($P = 0.046$). Furthermore, the *MET* mutations found were predominantly non-*MET* Δ ex14,

including some mutations with unclear oncogenic potential (*MET*^{A179T}, *MET*^{N375S}, and *MET*^{T1010I}) (Supplemental Figure 2A). We next looked at our Caris cohort, which did not include these *MET* variants. There was a significantly increased number of *MET* mutations, the majority of which were *MET* Δ ex14, in the primary lung compared with extracranial metastatic sites (non-BMs) or BMs (Supplemental Figure 4A and Supplemental Table 5). Notably, we did not detect any *MET* Δ ex14 in our BM cohort. Interestingly, we did find a statistically higher tumor mutational burden in BMs (median 11 mut/Mb) compared with extracranial metastases (median 8 mut/Mb, $P < 0.0001$) or lung (median 7 mut/Mb, $P < 0.0001$) in the Caris cohort (Supplemental Figure 4B).

MET-altered BMs are genomically distinct from non-*MET*-altered BMs. We next compared *MET*-altered (mutations and amplifications) LUAD BMs ($N = 31$) to non-*MET*-altered BMs ($N = 43$). *VHL* mutations were the only alterations that were significantly enriched in *MET*-altered BMs (16% vs. 0%, $P = 0.01$), with all identified *VHL* mutations co-occurring with *MET* mutations (Figure 5). Other genes that were more frequently mutated in *MET*-altered LUAD BMs but did not reach statistical significance included *CDKN2A* (16% vs. 7%; $P = 0.19$), *RET* (16% vs. 9%; $P = 0.29$), *ABL1* (13% vs. 2%; $P = 0.09$), *IDH1* (10% vs. 0%; $P = 0.07$), and *ALK* (10% vs. 5%; $P = 0.35$). Conversely, genes that were less fre-

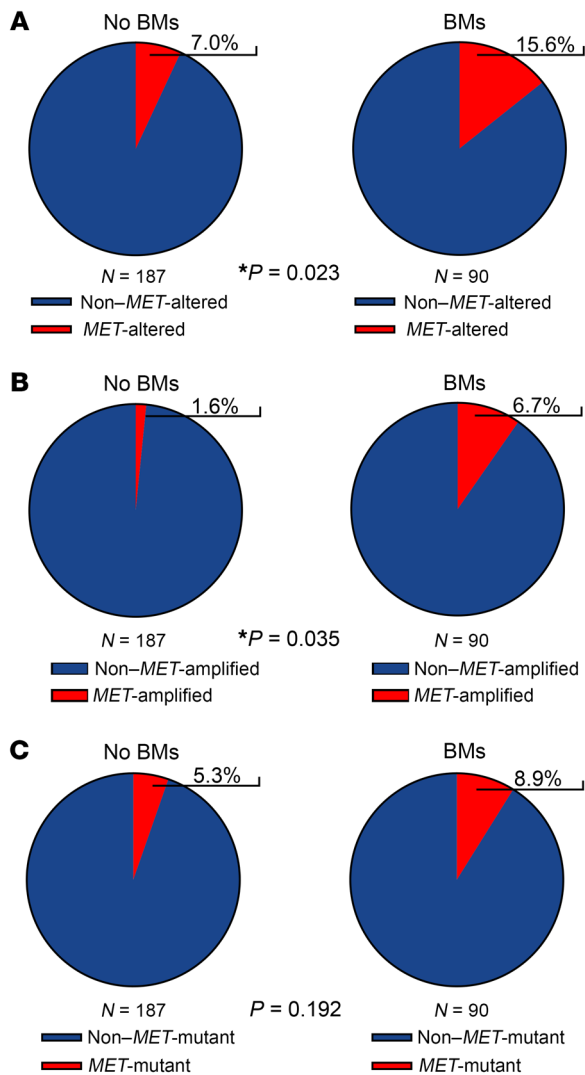


Figure 3. *MET* alterations detected in ctDNA are found more often in patients with BMs. (A) Percentage of ctDNA-positive *MET* alterations (amplifications and mutations combined) in patients with ($N = 90$) and without ($N = 187$) BMs, as detected with the Guardant360 CDx assay. (B) Percentage of ctDNA-positive *MET* amplifications in patients with ($N = 90$) and without ($N = 187$) BMs, as detected with the Guardant360 CDx assay. (C) Percentage of *MET* mutations in patients with ($N = 90$) and without ($N = 187$) BMs. Fisher's exact test, 1-sided; P values are shown for each comparison.

quently mutated in *MET*-altered cases included *ATM*, *JAK3*, and *KDR*. Of note, *KRAS*^{Q61X} variants were significantly more common in *MET*-altered BMs compared with non-*MET*-altered BMs (16% vs. 2%, $P = 0.04$) (Supplemental Figure 5E). Interestingly, while genes such as *ALK*, *APC*, *FGFR3*, *IDH1*, *RB1*, and *SMAD4* were not significantly different between *MET*-altered and non-*MET*-altered BMs, they were enriched in cases with *MET* mutations compared with those with *MET* amplifications. Notably, *VHL*, *ALK*, *IDH1*, and *FGFR2* alterations were completely absent in the *MET*-amplified samples. *MET*-amplified BMs were associated with a significantly lower variant number compared with *MET* mutant BMs in our cohort (2.57 median variants per BM vs. 13.8 median variants per BM, $P = 0.0006$). The gene variants that exhibited significant

differences are shown in Supplemental Figure 5. The complete list of variants for all non-*MET*-altered and *MET*-altered LUAD BM cases is shown in Supplemental Tables 6 and 7. These data suggest that *MET*-altered BMs, especially *MET*-amplified BMs, represent a molecularly and biologically distinct subset of BMs.

BMs have distinct transcriptomic profiles of altered immune and metabolic signatures compared with primary LUAD. To investigate transcriptomic differences between primary LUAD and LUAD BMs, we performed RNA-seq on 5 matched cases. Differential gene expression analysis identified 174 genes that were significantly differentially expressed between primary LUAD and matched BM samples (FDR = 0.05, fold change ≥ 2.0 or ≤ -2.0) (Figure 6A, ordered by group; Supplemental Figure 6, ordered by patient; Supplemental Tables 8–10). We conducted GSEA (Ensembl) using MSigDB Hallmark gene sets on the RNA-seq data from the matched samples. The top 20 pathways that were significantly up- or downregulated in LUAD BMs compared with primary LUAD are shown in Figure 6B and Supplemental Table 11. As expected (52–54), several immune-related signatures were significantly downregulated in LUAD BMs, including allograft rejection, IFN- γ response, IL-6/JAK/STAT3 signaling, inflammatory response, TNF- α signaling via NF- κ B, IFN- α response, and IL-2/STAT5 signaling. The suppression of these pathways suggests diminished immune activation and cytokine signaling in the brain metastatic microenvironment, which may facilitate immune evasion and metastatic progression. The downregulation of key inflammatory and immune-mediated pathways, such as TNF- α signaling and IFN responses, indicates potential reduced proinflammatory signaling, which could be critical for the survival of LUAD cells in the brain microenvironment. To further examine immune differences between primary LUAD and BMs, we conducted immune cell subset analysis on the matched cases (Supplemental Figure 6B). In all cases, the microenvironment and immune score as well as specific immune cell types, including B cells and dendritic cells, were significantly reduced in the LUAD BMs compared with primary LUAD, indicating that BMs exhibit immune-tolerant characteristics.

Previous studies, primarily in melanoma and breast BMs, demonstrated that oxidative phosphorylation (OXPHOS) is commonly used in BMs (55, 56). As expected, OXPHOS was among the most significantly upregulated pathways in LUAD BMs; however, there was also a smaller but significant increase in glycolysis. Additionally, the upregulation of Myc targets could further indicate metabolic adaptation in the brain microenvironment. This pathway enrichment results were confirmed through fast GSEA (fGSEA; classical GSEA algorithm) (Supplemental Figure 7A and Supplemental Table 12).

MET-amplified BMs have a distinct transcriptomic profile and immune landscape from non-MET-amplified BMs. We next sequenced *MET*-amplified ($N = 11$) versus non-*MET*-amplified ($N = 23$) LUAD BMs and identified 243 genes that were significantly differentially expressed between these groups (Figure 6C and Supplemental Tables 13–15). Notably, a single *MET*-amplified case with the lowest amplification (*MET*/*CEP* = 2.15) clustered with the non-*MET*-amplified cases. Ensembl GSEA and fGSEA of the BM cases showed significant upregulation or modulation of immune-related processes (IFN- α and IFN- γ responses, allograft rejection, IL-6/STAT3 signaling, IL-2/STAT5 signaling, and TNF- α signal-

Table 3. Selected patient characteristics for UPMC NGS cohort

	Primary LUAD, N = 180	BMs, N = 74	P value ^a
Age at diagnosis in yrs, mean (± SD) range	68.1 (± 9.2) 44–87	60.9 (± 9.2) 37–80	NS
Sex, N (%)			
Male	81 (45.0)	45 (60.8)	0.02
Female	99 (55.0)	29 (39.2)	
Race, N (%)			
White	168 (93.3)	68 (91.9)	NS
Black/African American	12 (6.7)	6 (8.1)	
American Indian/Alaska Native	0	0	
Asian	0	0	
Unknown ^b	0	0	
Smoking status, N (%)			
Ever	166 (92.2)	74 (100.0)	0.004
Never	14 (7.8)	0	
Stage, N (%)			
I–II	150 (83.3)	0	NA
III	24 (13.4)	0	
IV	6 (3.3)	74 (100)	NA
Metastases, N (%)			
Brain			
Synchronous	4 (2.2)	46 (62.2)	NA
Metachronous	148 (82.2)	0	
Liver			
Synchronous	0	1 (1.4)	NA
Metachronous	5 (2.8)	4 (5.4)	
None	175 (97.2)	69 (93.2)	
Unknown	0	0	
Alive at last follow-up	25 (13.9)	1 (1.4)	0.002

^a χ^2 test was used to determine P values. ^bNo data available.

ing via NF- κ B), cell cycle regulation and proliferation (E2F targets, G₂M checkpoint, mitotic spindle, Myc targets, KRAS signaling, and mTORC1 signaling), metabolic pathways (adipogenesis, glycolysis, and heme metabolism), pathways involved in EMT (apical junction, apical surface, and EMT), and coagulation pathways in *MET*-amplified BM compared with non-*MET*-amplified BM cases (Figure 6D, Supplemental Figure 7B, and Supplemental Tables 16 and 17).

We have previously shown that the EMT transcription factor *TWIST1* is a downstream target of the HGF/*MET* pathway, is required for *MET* tumorigenesis, and mediates *MET* TKI resistance (47, 57, 58). In support of its relevance in BMs, in the BM tumor microenvironment (TME), astrocytes have been shown to induce *TWIST1* in BMs, leading to chemoresistance (59), and a prior study reported *TWIST1* mRNA and protein expression in approximately 70% of BMs across breast, lung, kidney, and colon cancers as well as increased *TWIST1* mRNA in a paired primary lung/BM (60). Given that we observed modulation of pathways involved in EMT, we evaluated whether *TWIST1* expression would be higher in our *MET*-amplified BM cases compared with non-*MET*-amplified cases. We performed *TWIST1* IHC in a subset of BM cases with available tissue. *TWIST1* was detected in 55% of the *MET*-amplified cases compared with only 21% of *MET* WT BM cases ($P = 0.047$) (Supplemental Figure 8). These findings extend prior reports of *TWIST1* involvement in BMs and support its association with *MET* pathway activation.

To further validate these findings, we utilized the Caris dataset to assess distinct immune cell populations and immune-oncology (IO) marker expression in *MET*-amplified, *MET*-altered (mutant and/or amplified), and non-*MET*-amplified/ altered BMs. We first examined the expression of several IO markers and found that programmed cell death protein 1 (PD-1) and PD-L1 were significantly increased in both *MET*-altered and -amplified BMs (Supplemental Figure 9A and Supplemental Figure 10A). The increased PD-L1 expression was confirmed by PD-L1 IHC (22C3 pharmDx; 50% *MET* WT vs. 80% *MET*-altered, $P < 0.001$; data not shown). PD-L2 was also elevated in both groups but reached statistical significance only in the *MET*-altered BM group (Supplemental Figure 9A). We did not observe a significant increase in either the IFN- γ or T cell inflamed signature in this dataset when we compared either the *MET*-altered or -amplified cohorts to the non-*MET*-amplified/ altered BM cohort (Supplemental Figure 9B and Supplemental Figure 10B). Conversely, in *MET*-altered BMs compared with non-*MET*-altered BMs, M1 macrophages were significantly elevated, whereas NK cells were significantly reduced (Supplemental Figure 9C). No differences were observed in other immune subsets, such as B cells, M2 macrophages, monocytes, neutrophils, CD4⁺ and CD8⁺ T cells, Tregs, or dendritic cells, between the groups. Similar trends were observed in *MET*-amplified BMs,

with a significant increase in M1 macrophages and a reduction in M2 macrophages. Additionally, NK cells and CD4 T cells were also decreased in *MET*-amplified BMs (Supplemental Figure 10C). Together, these findings suggest a shift in the immune landscape toward a less immunosuppressive microenvironment in *MET*-driven BMs, characterized by altered immune cell composition and elevated immune checkpoint markers, potentially contributing to an inflamed phenotype in these tumors.

Lung cancer patients with *MET*-amplified BMs have poor OS. Finally, we asked if the presence of a *MET* amplification in LUAD BMs had any prognostic significance. We analyzed OS from the time of initial lung cancer diagnosis in patients with *MET*-amplified BMs compared with those with non-*MET*-amplified BMs using data from the Caris dataset. Our findings demonstrate that patients with *MET*-amplified BMs ($N = 22$) exhibit significantly poorer OS compared with those without *MET* amplification ($N = 1,039$) (Figure 7A). At 1 year, the survival rate for patients with *MET*-amplified BMs was 63%, decreasing to 23% at both 3 and 5 years. In contrast, patients without *MET* amplification had higher survival rates, with 81% at 1 year, 65% at 3 years, and 51% at 5 years. Median OS was 16.4 months in the *MET*-amplified cohort and 61.4 months in the non-*MET*-amplified cohort (HR: 2.05; $P = 0.006$). This 3.7-fold difference in OS highlights the aggressive nature of *MET*-amplified tumors, which may drive a more rapid progression and poorer prognosis, particularly after BMs

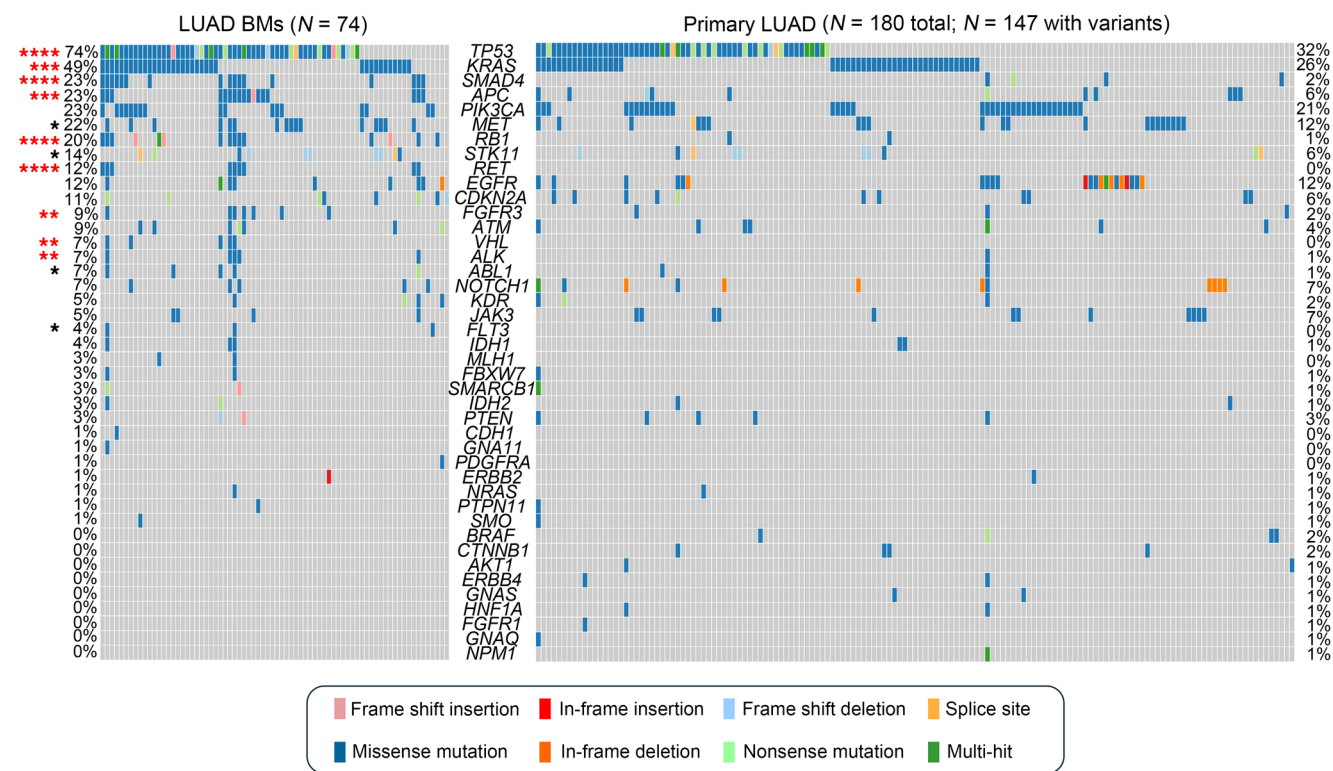


Figure 4. LUAD BMs have a distinct mutational profile compared with primary LUAD tumors. OncoPrint of the distribution of mutations for patients with LUAD BMs ($N = 74$) compared with those with primary LUAD tumors ($N = 180$ total; $N = 147$ with variants detected). Frequency of mutations is listed for each gene in order of the highest to lowest frequency in LUAD BMs. The mutation types are color-coded and annotated in the key. Variants annotated as “Multi-hit” are genes that are mutated more than once in the same sample. Fisher’s exact test, 2-sided; * $P \leq 0.05$, ** $P \leq 0.01$, *** $P \leq 0.001$, **** $P \leq 0.0001$. Red asterisks indicate significance after FDR adjustment. A q value < 0.05 was considered significant.

occur. Of note, this difference was still significant when patients with an *EGFR* mutant and co-occurring *MET* amplification were excluded (Figure 7B). The significantly shorter OS in patients with *MET*-amplified BMs underscores the aggressive nature of *MET*-driven BMs and suggests a need for novel therapeutic strategies targeting *MET* to improve outcomes for this patient subgroup.

Discussion

Advances in targeted therapies and immunotherapy have dramatically improved the management of NSCLC, leading to better control of extracranial disease and prolonged survival. These agents have transformed the treatment landscape, allowing patients with NSCLC to live longer with controlled systemic disease. However, as survival increases, more patients develop BMs over the course of their disease. Treatment options for BMs include stereotactic radiosurgery, whole-brain radiation therapy, surgery in select cases, and systemic therapies with CNS penetration, such as osimertinib for *EGFR* mutant NSCLC and alectinib or lorlatinib for *ALK*-rearranged disease. Despite these advances, BMs remain a major clinical challenge for patients with lung cancer, underscoring the need for more effective CNS active therapies and prevention strategies.

In this study, we found *MET* amplification in 16% of resected LUAD BMs, even when it was not present in biopsies from extracranial sites. These amplification events were not acquired after treatment with targeted therapy and were primarily observed in BMs without targetable oncogenic drivers, representing what we believe

to be a unique and potentially actionable population of patients with BMs, including those whose extracranial disease lacks a defined oncogenic driver. Importantly, several studies have demonstrated the CNS activity of the FDA-approved *MET* TKIs capmatinib and tepotinib as well as their respective efficacy against *MET*-amplified NSCLC (31, 35–38). Thus, identification of *MET* amplifications in BMs of NSCLC could expand the treatment options available to these patients, even when the primary tumor is *MET* negative. This study also reveals several limitations of the current approach used to detect molecular alterations. Prior studies examining BM-specific or -enriched alterations were dependent upon NGS technologies, which may greatly underestimate amplification rates given the need for higher cutoffs and strict algorithms to account for aneuploidy in copy number determination. In our study, we found a statistically significant increase in *MET* amplification in BMs compared with primary NSCLC or non-BM sites using the Caris NGS platform; however, the absolute percentage was significantly lower than what was observed utilizing FISH. Similarly, we previously found a statistically significant increase in *MET* amplification in BMs compared with primary lung tumors using Foundation Medicine’s dataset (4.4% [133/3,035] vs. 2.3% [170/7,277]) ($P < 0.0001$) (45). Interestingly, prior studies have demonstrated that a much lower level of *MET* amplification is needed to predict response to *MET*-targeted therapy when measured by FISH ($MET/CEP7 \geq 4$) rather than by NGS ($GCN \geq 10$) (32–34), and a range of amplification ratios have been reported to predict response to *MET* TKIs when detected

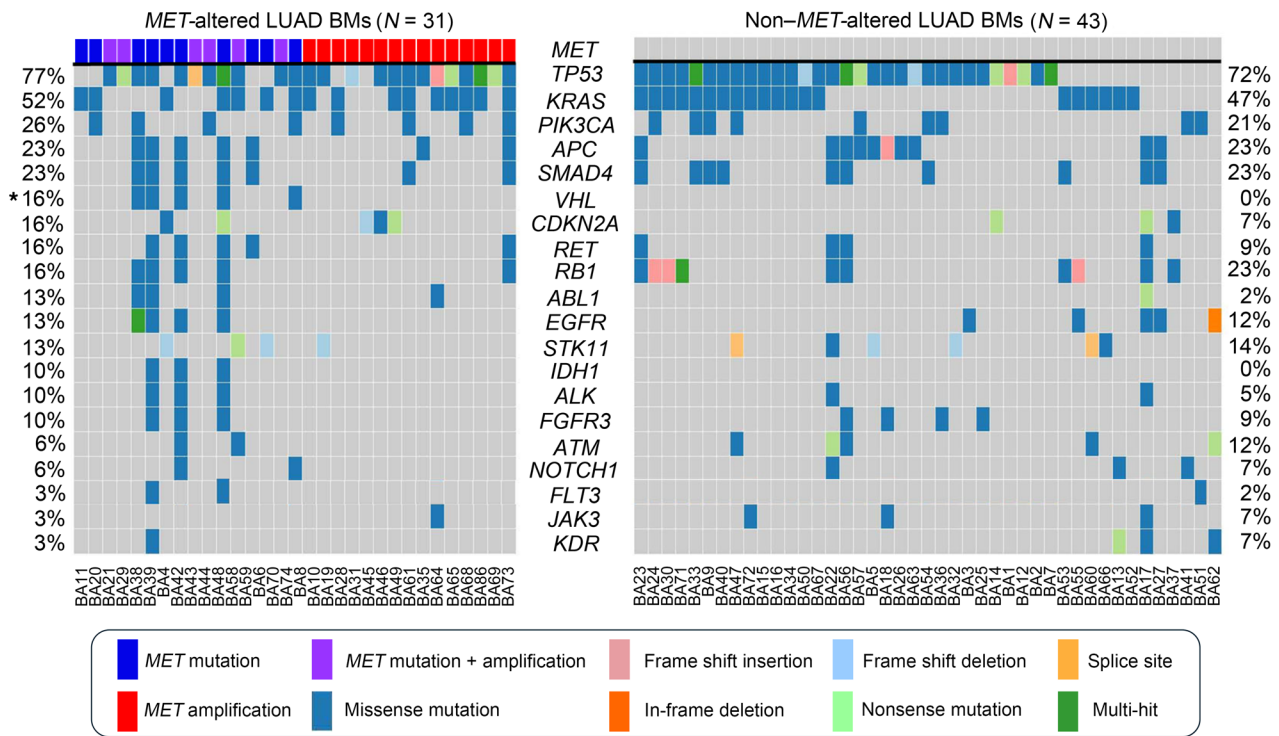


Figure 5. MET-altered BMs are genomically distinct from non-MET-altered BMs. OncoPlot of the distribution of mutations for patients with MET altered LUAD BMs (N = 31) compared with those with non-MET-altered LUAD BMs (N = 43). Frequency of mutations is listed for each gene in order of highest to lowest. The mutation types are color-coded and annotated in the key. Variants annotated as “Multi-Hit” are genes that are mutated more than once in the same sample. Fisher’s exact test, 1-sided; *P ≤ 0.05.

by blood-based ctDNA assays (36, 61, 62). Despite the approval of multiple MET TKIs and other MET-directed targeted therapies in late-phase trials, the gold standard for detecting MET amplification in the clinic is still widely debated (18). Our findings suggest that the standard NGS approach is inadequate.

This study, along with several previously published studies, reinforces the notion that molecular testing performed on extracranial tissue is often a poor predictor of potential targetable alterations in the CNS. Prior studies demonstrated that BM-specific HER2 amplification is found in patients with breast cancer who have HER2-negative extracranial disease (43, 63). Similarly, BM-specific copy number alterations have been identified in patients with lung cancer (44). As more BM-specific targetable alterations are identified, there is a critical need for better detection of BM-specific or -enriched alterations. Prior studies utilizing blood-based ctDNA-based assays have shown only modest performance in detecting BM-enriched or -specific alterations; some studies have suggested a better diagnostic yield from the use of relatively invasive lumbar punctures to obtain cerebrospinal fluid-derived (CSF-derived) ctDNA for detecting CNS-specific alterations (49–51). Previous studies focused primarily on patients with LUAD who had leptomeningeal disease showed that MET amplification is detectable and often present in the CSF, even in EGFR WT patients (64–66). Of note, in our current study, BMs were associated with an increased likelihood of having a MET amplification or MET mutation by ctDNA. This suggests that blood-based ctDNA assays may be capable of detecting a significant fraction of MET amplification in BMs; however, this needs to be confirmed in a prospective study. A limitation of our

study is the limited overlap between the ctDNA and FISH cohorts, with only 4 patients having both blood and brain tissue available, which precluded a direct comparison of MET status between blood and tissue. Alternatively, radiomic approaches have been used on CT images of pulmonary nodules to predict mutational subtypes in NSCLC (67) and on brain MRI images to detect mutational subtypes in glioblastoma (68, 69) and EGFR or KRAS mutations in lung cancer BMs (70–74). It is possible that a radiomic approach could be used to detect BM-specific alterations such as MET amplifications.

In contrast to published data showing that the HGF/MET pathway promotes an extracranial immunosuppressive TME (75–83), our findings suggest that MET-amplified BMs have a more inflammatory transcriptional signature, along with increased expression of PD-1 and PD-L1, and significant upregulation or modulation of immune-related processes (IFN-α and IFN-γ responses, allograft rejection, IL-6/STAT3 signaling, IL-2/STAT5 signaling, and TNF-α signaling via NF-κB) compared with non-MET-amplified BM cases. Of note, the IL-6/JAK/STAT3 pathway was increased in MET-amplified BM compared with non-MET-amplified BM cases. Prior studies in extracranial disease have suggested that MET/STAT3 signaling is associated with immune evasion via M2 macrophage polarization, myeloid-derived suppressor cell (MDSC) expansion, and increased cancer-associated fibroblast signaling leading to MDSC migration (75, 84–88). Although we did not observe any evidence of an increased activated T cell population, there was a notable increase in M1 macrophages and a corresponding decrease in M2 macrophages, suggesting a potentially less immunosuppressive TME. As such, it is possible that utilizing

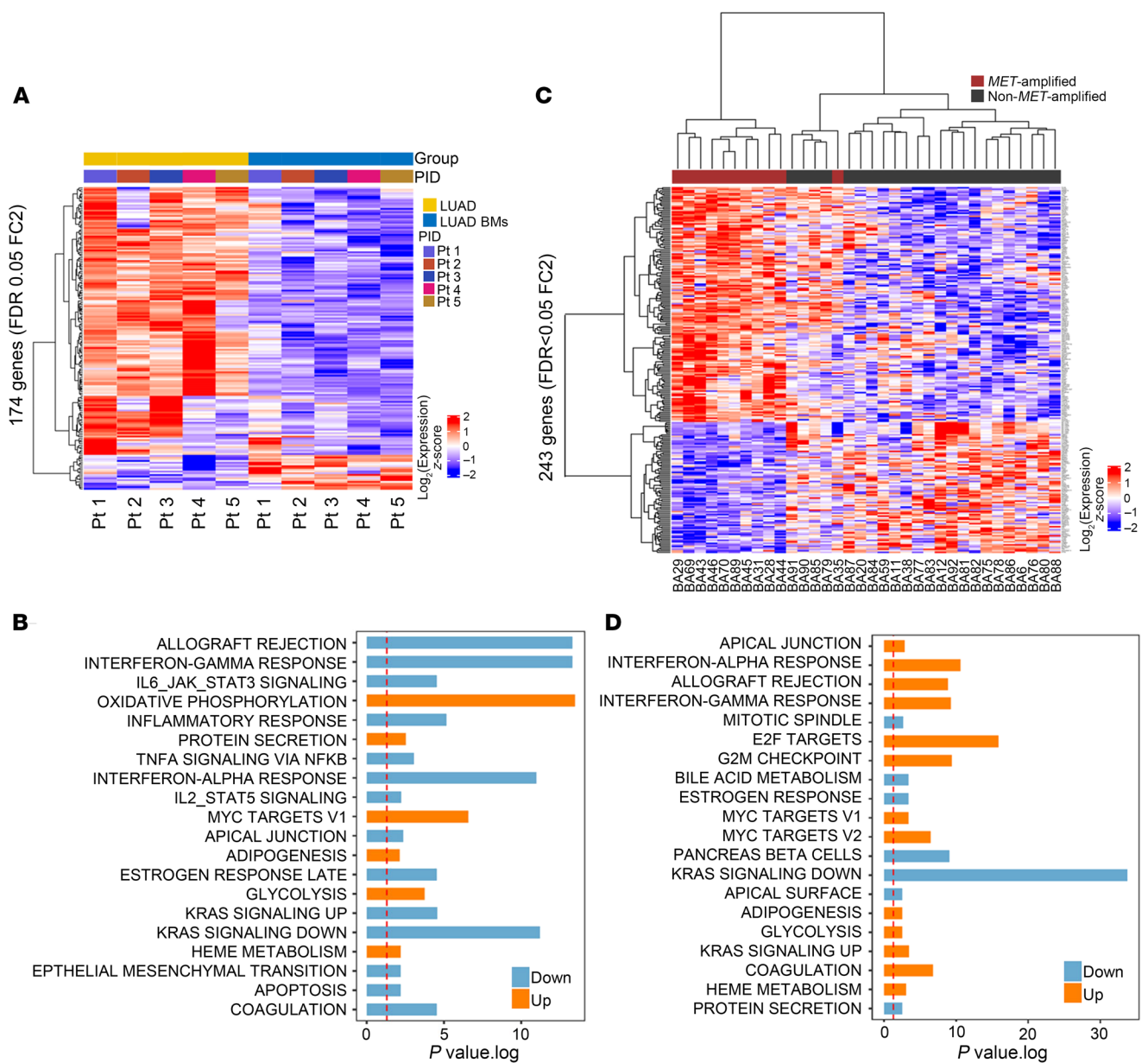


Figure 6. LUAD BMs have a distinct transcriptional profile compared with matched primary LUAD tumors, and *MET*-amplified BMs are distinct from non-*MET*-amplified BMs. (A) Heat map of 174 differentially expressed genes in 5 matched primary LUAD (yellow) and BMs (blue) (FDR < 0.05, fold change [FC] ≥ 2.0 or ≤ -2.0). **(B)** GSEA of the Hallmark gene sets from the Molecular Signatures Database (MSigDB) showing increased (orange) and decreased (blue) pathways in BMs compared with primary LUAD. The top 20 pathways are shown sorted by median rank of higher to lower (representing confidence higher to lower). **(C)** Heat map of 243 differentially expressed genes in *MET*-amplified (red) and *MET* WT (black) BMs (FDR < 0.05, fold change ≥ 2.0 or ≤ -2.0). **(D)** GSEA of the Hallmark gene sets from the MSigDB showing increased (orange) and decreased (blue) pathways in *MET*-amplified compared with non-*MET*-amplified BMs. The top 20 pathways are shown sorted by median rank of higher to lower (representing confidence higher to lower). The red dashed lines in **B** and **D** represent the threshold of what was considered significant.

MET inhibitors for *MET*-amplified BMs may have the unintended effect of suppressing immune responses. It is also possible that this inflammatory brain microenvironment could make *MET*-amplified BMs more sensitive to immunotherapy; however, these hypotheses require both preclinical and clinical validation. A future direction is also to investigate whether upregulation of STAT3 signaling in *MET*-amplified BMs leads to a more immunosuppressive TME. Notably, previous studies of molecularly unselected LUAD BM patients demonstrated modest but consistent CNS activity of the

anti-PD-1 agent pembrolizumab or the combination of the anti-CTLA-4 ipilimumab and the anti-PD-1 agent nivolumab (89–91).

Interestingly, we found unexpected metabolic differences in *MET*-amplified BMs. While previous studies have demonstrated that melanoma and breast cancer BMs primarily utilize OXPHOS regardless of the metabolic pathways used extracranially (55, 56), we observed increased glycolysis in our *MET*-amplified BMs. We saw increased OXPHOS in our LUAD BM versus LUAD lung samples consistent with these prior studies. However, it appears that

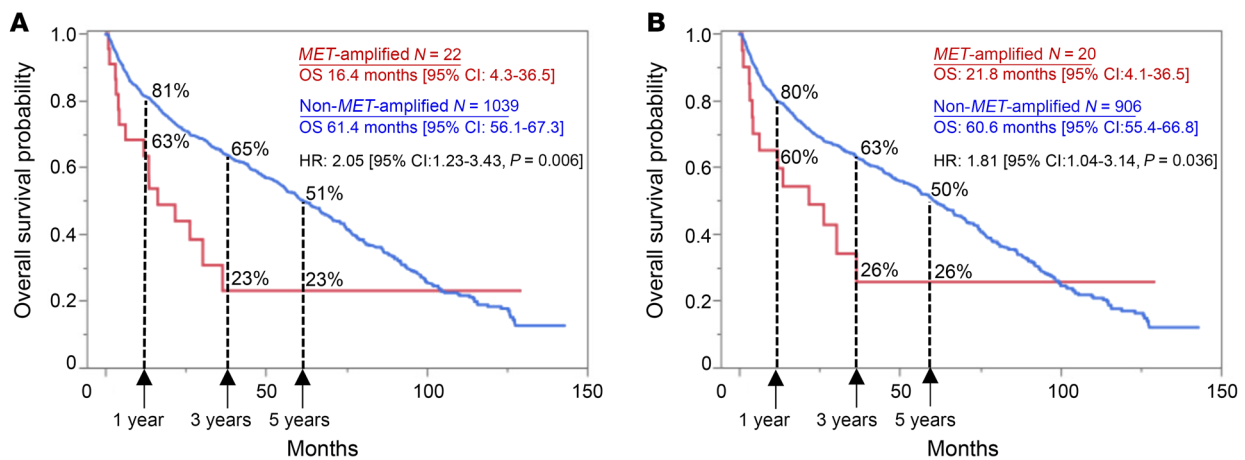


Figure 7. Patients with NSCLC *MET*-amplified BMs have worse OS. Kaplan-Meier survival analysis showing OS in months from initial diagnosis in patients with NSCLC BMs stratified by *MET* amplification (red line) versus no amplification (blue line). Median OS in months, HR, and CI were calculated. (A) All patients; (B) all patients excluding those with *EGFR* mutations. 1-, 3-, and 5-year survival rates are indicated.

MET-amplified BMs, which utilized primarily glycolysis, are distinct from non-*MET*-amplified BMs. Interestingly, prior cell line studies have demonstrated that *MET* is a major driver of glycolysis, at least extracranially (92–94). Notably, several glycolysis inhibitors, such as 2-deoxy-glucose (2DG) and PFK158, with CNS penetration, have been tested in early-phase trials (95, 96). Additionally, newer 2DG analogs, such as WP1122, have been developed with an increased half-life and enhanced blood-brain barrier penetration (97). Finally, newer agents, such as BPM31510 (ubidecarenone), which induced a metabolic switch from glycolysis to OXPHOS, have shown promising results preclinically and in early-phase trials as well (98–106). It is possible that these glycolytic inhibitors could be another therapeutic strategy for targeting *MET*-amplified BMs. Furthermore, as increased lactate in the TME due to *MET*-driven glycolysis extracranial appears to contribute to an immunosuppressive TME (75), it is possible that combinations examining glycolytic inhibitors with immunotherapy agents may be effective against *MET*-amplified BMs as well.

Mechanistically, we have previously shown that the EMT transcription factor *TWIST1*, which has been implicated in BMs (59, 60), is essential for *MET*-driven tumorigenesis (47, 57, 58), is regulated by the HGF/*MET* signaling axis (47), and can confer resistance to *MET* TKIs (47). *TWIST1* has also been shown to suppress apoptosis by downregulating proapoptotic factors (e.g., BIM) (107). These findings suggest that *TWIST1* may mediate a dual pro-survival and prometastatic program through both suppression of apoptosis and induction of EMT in an HGF/*MET*-dependent manner. Our findings that *TWIST1*-positive BMs were more likely to be *MET* amplified also suggests a mechanistic link between *TWIST1* expression and activation of the *MET* pathway in metastatic progression to the brain. A future direction is to further evaluate the functional role of *TWIST1* in *MET*-amplified BMs.

Our studies suggest that the hypoxia-inducible factor 1- α (HIF-1 α) pathway may be important for BMs as *VHL* mutations were only found in BMs and not primary LUAD. Interestingly, we also found that *VHL* mutations were exclusively present in *MET* mutant BMs but absent in *MET*-amplified BMs. Prior studies have shown that hypoxia increases *MET* expression via HIF-1 α and that *MET*

increases HIF-1 α protein levels (108–110). Furthermore, coexpression of high *MET* and HIF-1 α has been reported in breast cancer (111). It is possible that some *MET* mutational variants are unable to sufficiently stabilize HIF-1 α ; thus, loss of *VHL* is necessary to drive HIF-1 α protein expression. A future direction is to examine whether the HIF-1 α transcriptional program is activated in *MET* mutant versus *MET*-amplified versus *MET* WT BMs.

While this study provides important insights into *MET* amplification in LUAD BMs, several limitations should be acknowledged. First, although our findings are based on well-annotated human specimens and validated in a large, independent patient cohort, the observational nature of clinical tissue-based research limits our ability to experimentally test mechanistic hypotheses. Second, not all patient cohorts utilized the same assay for detection of *MET* amplification (FISH vs. NGS) nor contained the same granularity of patient data, which made it difficult to integrate datasets. Third, our current study focuses on detectable genetic alterations in *MET* leading to its overexpression and activation, but a recent study has suggested that upregulation of mesothelin (*MSLN*) is a nongenomic mechanism of *MET* activation in BMs (112). Interestingly, our RNA-seq data showed increased *MSLN* mRNA in BM versus primary LUAD samples, but it was decreased in *MET*-amplified BMs compared with non-*MET*-amplified BMs, suggesting that *MET* amplification and high *MSLN* mRNA expression are mutually exclusive. Finally, while we identified immune, metabolic, and mutational changes associated with *MET* alterations, the functional consequences of these changes have not yet been directly tested in preclinical model systems. Future studies utilizing genetically engineered mouse models, in vivo metastases models, organotypic brain slice cultures, and targeted functional perturbations are essential to define the mechanistic role of *MET* amplification and its downstream signaling networks in LUAD BM biology. Nonetheless, these findings provide a critical foundation for understanding *MET*-altered BMs and offer strong rationale for development of targeted *MET* therapies in patients with LUAD BMs.

In conclusion, the increasing incidence of BMs underscores the need for deeper characterization to uncover novel therapeutic

strategies. Our findings identified a significant enrichment of *MET* amplification in oncogene driver–negative LUAD BMs, independent of prior targeted therapy, indicating that this was not merely a consequence of acquired resistance. Additionally, our study found a distinct molecular and transcriptomic landscape in LUAD BMs, shaped by unique immune and metabolic adaptations and induction of an EMT program that distinguished primary LUAD from LUAD BMs as well as *MET*-altered BMs from non-*MET*-altered BMs. Furthermore, patients with *MET*-amplified BMs had significantly worse survival. Finally, our findings suggest that targeting *MET* amplification could present a therapeutic opportunity for a large subset of patients with LUAD BMs. Prospective trials validating ctDNA for *MET* detection and combining *MET* TKIs with glycolysis inhibitors or immunotherapy are warranted.

Methods

Sex as a biological variable. Our study cohort included both male and female patients with LUAD; the sex distribution is reported in Tables 1–3. In the *in vivo* experiment, only female mice were used. This choice was based on prior findings from our group demonstrating more consistent tumor establishment in female mice. While this approach reduced biological variability, we acknowledge the limitation of using a single sex and will incorporate both male and female animals in future studies.

Statistics. For the *in vivo* PDX experiment, a 2-sided Student's *t* test was performed on the final tumor volume between the control and capmatinib treatment groups. Bioluminescent imaging data from the *in vivo* experiment were analyzed using the Mann-Whitney test. A 2-sided Fisher's exact test was used to determine significant differences in *MET* amplification by tumor type, in mutations found in primary LUAD versus BMs and *MET*-altered LUAD BMs versus non-*MET*-altered BMs. *P* values were adjusted for an FDR of 0.05 using the Benjamini-Hochberg method. *P* values of less than 0.05 were considered significant. A Fisher's exact test was also performed when evaluating specific gene variants shown in Supplemental Figures 2, 3, and 5 and to compare the frequency of ctDNA *MET* alterations, including *MET* amplifications and mutations, in individuals with and without BMs. A χ^2 test was used to determine if there was a statistically significant difference in the rate of metastatic disease to the brain in the focally *MET*-amplified versus nonfocally *MET*-amplified BMs and for differences in patient characteristics in Tables 1–3. Survival curves were estimated using the Kaplan-Meier method.

Study approval. This study was conducted under University of Pittsburgh IRB protocol 12070229 and STUDY19110031. Patient tissue to generate the PDX model was obtained from patients undergoing standard-of-care craniotomy after informed consent under University of Pittsburgh IRB protocol 19080321. Animal studies were approved and conducted under University of Pittsburgh IACUC protocol 21089597.

Data availability. RNA-seq data FASTQ files (*N* = 40) were deposited in the National Center for Biotechnology Information Sequence Read Archive database (accession number PRJNA1129590). Additional details regarding data and protocols that support the findings of this study are available from the corresponding authors upon request. Values for all data points in the graphs are provided in the Supporting Data Values file. All remaining materials and methods are described in Supplemental Methods.

Author contributions

Conception and design, methodology, and funding acquisition: TFB, SD, and LPS. Data acquisition: TFB, SD, MAV, EM, AS, SB, AGD, PD, JJ, VK, JX, and LPS. Data analysis and interpretation of data: TFB, SD, AC, JX, URC, RB, CT, and LPS. Writing (original draft): LPS and TFB. Writing (review and editing): TFB, SD, AC, EM, MAV, AS, SB, AGD, PD, JJ, VK, AP, JX, MO, MJG, SA, URC, RB, CT, and LPS.

Funding support

This work is the result of NIH funding, in whole or in part, and is subject to the NIH Public Access Policy. Through acceptance of this federal funding, the NIH has been given a right to make the work publicly available in PubMed Central.

- National Cancer Institute (R01 CA244270-01A1 to TFB and LPS).
- Department of Defense LCRP-IITRA (W81XWH-22-1-0350 to TFB and LPS).
- National Cancer Institute (P50CA090440 to TFB, LPS, and SD).
- American Cancer Society Research Scholar Award (RSG TBG – 132939 to TFB, LPS, and SD).
- The University of Pittsburgh Institute for Precision Medicine (to TFB and LPS).
- Libby's Lungs (to LPS).
- We Wish Foundation (to TFB).
- National Cancer Institute grant (P30CA047904) awarded to the UPMC Hillman Cancer Center–supported research reported in this publication using the Biostatistics Facility (RRID: SCR025355), Cancer Bioinformatics Services (RRID: SCR025356), Cancer Genome Facility (RRID: SCR025357), In Vivo Imaging Facility (RRID: SCR025360), and Animal Facility (RRID: SCR025152).
- Lung Cancer Research Foundation and MET Crusaders Research Grant on MET-Driven Lung Cancer (to TFB and LPS).

Acknowledgments

The authors thank Angela Dahlberg (The Ohio State University Comprehensive Cancer Center Division of Medical Oncology, Columbus, Ohio) for editing this manuscript.

Address correspondence to: Timothy F. Burns, The Ohio State University, 460 W. 12th Ave., Biomedical Research Tower, Suite 596, Columbus, Ohio 43210, USA. Phone: 614.366.5154; Email: timothy.burns@osumc.edu. Or to: Laura P. Stabile, UPMC Hillman Cancer Center, 5118 Centre Avenue, Research Pavilion Office 2.18d, Pittsburgh, Pennsylvania 15232, USA. Phone: 412.623.2015; Email: stabilela@upmc.edu.

TFB's present address is: Division of Medical Oncology, Department of Internal Medicine, The Ohio State University Comprehensive Cancer Center, Columbus, Ohio, USA.

SD's present address is: Department of Pathology, Yale School of Medicine, New Haven, Connecticut, USA.

MAV's present address is: Department of Medicine, UCLA, Los Angeles, California, USA.

AS's present address is: Department of Medicine, University of North Carolina, Chapel Hill, North Carolina, USA.

1. Siegel RL, et al. Cancer statistics, 2025. *CA Cancer J Clin*. 2025;75(1):10–45.
2. Berghoff AS, et al. Descriptive statistical analysis of a real life cohort of 2419 patients with brain metastases of solid cancers. *ESMO Open*. 2016;1(2):e000024.
3. Nayak L, et al. Epidemiology of brain metastases. *Curr Oncol Rep*. 2012;14(1):48–54.
4. Suh JH, et al. Current approaches to the management of brain metastases. *Nat Rev Clin Oncol*. 2020;17(5):279–299.
5. Moro-Sibilot D, et al. Non-small cell lung cancer patients with brain metastases treated with first-line platinum-doublet chemotherapy: analysis from the European FRAME study. *Lung Cancer*. 2015;90(3):427–432.
6. Sperduto PW, et al. Graded Prognostic Assessment (GPA) for patients with lung cancer and brain metastases: initial report of the small cell lung cancer GPA and update of the non-small cell lung cancer GPA including the effect of programmed death ligand 1 and other prognostic factors. *Int J Radiat Oncol Biol Phys*. 2022;114(1):60–74.
7. Sorensen JB, et al. Brain metastases in adenocarcinoma of the lung: frequency, risk groups, and prognosis. *J Clin Oncol*. 1988;6(9):1474–1480.
8. Cagney DN, et al. Incidence and prognosis of patients with brain metastases at diagnosis of systemic malignancy: a population-based study. *Neuro Oncol*. 2017;19(11):1511–1521.
9. Gainor JF, et al. The central nervous system as a sanctuary site in ALK-positive non-small-cell lung cancer. *J Thorac Oncol*. 2013;8(12):1570–1573.
10. Goldberg SB, et al. Pembrolizumab for management of patients with NSCLC and brain metastases: long-term results and biomarker analysis from a non-randomised, open-label, phase 2 trial. *Lancet Oncol*. 2020;21(5):655–663.
11. Wu XC, et al. The emerging role of immune checkpoint blockade for the treatment of lung cancer brain metastases. *Clin Lung Cancer*. 2024;25(6):483–501.
12. Benedettini E, et al. Met activation in non-small cell lung cancer is associated with de novo resistance to EGFR inhibitors and the development of brain metastasis. *Am J Pathol*. 2010;177(1):415–423.
13. Breindel JL, et al. EGF receptor activates MET through MAPK to enhance non-small cell lung carcinoma invasion and brain metastasis. *Cancer Res*. 2013;73(16):5053–5065.
14. Sakamoto S, et al. New metastatic model of human small-cell lung cancer by orthotopic transplantation in mice. *Cancer Sci*. 2015;106(4):367–374.
15. Yamada T, et al. Immunohistochemistry with antibodies to hepatocyte growth factor and its receptor protein (c-MET) in human brain tissues. *Brain Res*. 1994;637(1-2):308–312.
16. Graveel CR, et al. MET: a critical player in tumorigenesis and therapeutic target. *Cold Spring Harb Perspect Biol*. 2013;5(7):a009209.
17. Sadiq AA, Salgia R. Inhibition of MET receptor tyrosine kinase and its ligand hepatocyte growth factor. *J Thorac Oncol*. 2012;7(16 suppl 5):S372–S374.
18. Guo R, et al. MET-dependent solid tumours - molecular diagnosis and targeted therapy. *Nat Rev Clin Oncol*. 2020;17(9):569–587.
19. Okuda K, et al. Met gene copy number predicts the prognosis for completely resected non-small cell lung cancer. *Cancer Sci*. 2008;99(11):2280–2285.
20. Onozato R, et al. Activation of MET by gene amplification or by splice mutations deleting the juxtamembrane domain in primary resected lung cancers. *J Thorac Oncol*. 2009;4(1):5–11.
21. Park S, et al. High MET copy number and MET overexpression: poor outcome in non-small cell lung cancer patients. *Histol Histopathol*. 2012;27(2):197–207.
22. Tachibana K, et al. Abnormality of the hepatocyte growth factor/MET pathway in pulmonary adenocarcinogenesis. *Lung Cancer*. 2012;75(2):181–188.
23. Engelman JA, et al. MET amplification leads to gefitinib resistance in lung cancer by activating ERBB3 signaling. *Science*. 2007;316(5827):1039–1043.
24. Sequist LV, et al. Osimertinib plus savolitinib in patients with EGFR mutation-positive, MET-amplified, non-small-cell lung cancer after progression on EGFR tyrosine kinase inhibitors: interim results from a multicentre, open-label, phase 1b study. *Lancet Oncol*. 2020;21(3):373–386.
25. The Cancer Genome Atlas Research Network. Comprehensive molecular profiling of lung adenocarcinoma. *Nature*. 2014;511(7511):543–550.
26. Seo JS, et al. The transcriptional landscape and mutational profile of lung adenocarcinoma. *Genome Res*. 2012;22(11):2109–2119.
27. Frampton GM, et al. Activation of MET via diverse exon 14 splicing alterations occurs in multiple tumor types and confers clinical sensitivity to MET inhibitors. *Cancer Discov*. 2015;5(8):850–859.
28. Awad MM, et al. MET exon 14 mutations in non-small-cell lung cancer are associated with advanced age and stage-dependent MET genomic amplification and c-Met overexpression. *J Clin Oncol*. 2016;34(7):721–730.
29. Paik PK, et al. Response to MET inhibitors in patients with stage IV lung adenocarcinomas harboring MET mutations causing exon 14 skipping. *Cancer Discov*. 2015;5(8):842–849.
30. Drilon A, et al. Antitumor activity of crizotinib in lung cancers harboring a MET exon 14 alteration. *Nat Med*. 2020;26(1):47–51.
31. Wolf J, et al. Capmatinib in MET exon 14-mutated or MET-amplified non-small-cell lung cancer. *N Engl J Med*. 2020;383(10):944–957.
32. Ou SH, et al. Activity of crizotinib (PF02341066), a dual mesenchymal-epithelial transition (MET) and anaplastic lymphoma kinase (ALK) inhibitor, in a non-small cell lung cancer patient with de novo MET amplification. *J Thorac Oncol*. 2011;6(5):942–946.
33. Caparica R, et al. Responses to crizotinib can occur in high-level MET-amplified non-small cell lung cancer independent of MET exon 14 alterations. *J Thorac Oncol*. 2017;12(1):141–144.
34. Camidge DR, et al. Crizotinib in patients with MET-amplified NSCLC. *J Thorac Oncol*. 2021;16(6):1017–1029.
35. Le X, et al. Tepotinib in patients (pts) with advanced non-small cell lung cancer (NSCLC) with MET amplification (METamp). *J Clin Oncol*. 2021;39(15 suppl):9021.
36. Le X, et al. Clinical response to tepotinib according to circulating tumor (ct) DNA biomarkers in patients with advanced NSCLC with high-level MET amplification (METamp) detected by liquid biopsy (LBx). *J Clin Oncol*. 2022;40(16 suppl):9121.
37. Schuler M, et al. Molecular correlates of response to capmatinib in advanced non-small-cell lung cancer: clinical and biomarker results from a phase I trial. *Ann Oncol*. 2020;31(6):789–797.
38. Paik PK, et al. Tepotinib in non-small-cell lung cancer with MET exon 14 skipping mutations. *N Engl J Med*. 2020;383(10):931–943.
39. Friese-Hamim M, et al. Abstract 3407: Anti-tumor activity of tepotinib in orthotopic models of lung cancer patient-derived brain metastases with MET amplification. *Cancer Res*. 2020;80(16 suppl):3407.
40. Shen L, et al. Prominent response to savolitinib monotherapy in high-grade fetal adenocarcinoma with MET amplification and concurrent brain metastasis: a case report. *Transl Lung Cancer Res*. 2024;13(6):1407–1413.
41. Blanc-Durand F, et al. Tepotinib efficacy in a patient with non-small cell lung cancer with brain metastasis harboring an HLA-DRB1-MET gene fusion. *Oncologist*. 2020;25(11):916–920.
42. Wang P, et al. Rapid response of brain metastasis to crizotinib in a patient with KLC1-ALK fusion and MET gene amplification positive non-small cell lung cancer: a case report. *Cancer Biol Med*. 2017;14(2):183–186.
43. Brastianos PK, et al. Genomic characterization of brain metastases reveals branched evolution and potential therapeutic targets. *Cancer Discov*. 2015;5(11):1164–1177.
44. Shih DJH, et al. Genomic characterization of human brain metastases identifies drivers of metastatic lung adenocarcinoma. *Nat Genet*. 2020;52(4):371–377.
45. Huang RSP, et al. Clinicopathologic and genomic landscape of non-small cell lung cancer brain metastases. *Oncologist*. 2022;27(10):839–848.
46. Liu M, et al. Genomic and immune landscape of non-small cell lung cancer brain metastases. *JCO Precis Oncol*. 2025;9:e2400690.
47. Kumar V, et al. TWIST1 is a critical downstream target of the HGF/MET pathway and is required for MET driven acquired resistance in oncogene driven lung cancer. *Oncogene*. 2024;43(19):1431–1444.
48. Mayba O, et al. Integrative analysis of two cell lines derived from a non-small-lung cancer patient—a panomics approach. *Pac Symp Biocomput*. 2014;11(11):75–86.
49. De Mattos-Arruda L, et al. Cerebrospinal fluid-derived circulating tumour DNA better represents the genomic alterations of brain tumours than plasma. *Nat Commun*. 2015;6:8839.
50. Ma C, et al. Detection of circulating tumor DNA from non-small cell lung cancer brain metastasis in cerebrospinal fluid samples. *Thorac Cancer*. 2020;11(3):588–593.
51. Wu J, et al. Cerebrospinal fluid circulating tumor DNA depicts profiling of brain metastasis in NSCLC. *Mol Oncol*. 2023;17(5):810–824.
52. Tsakonas G, et al. An immune gene expression signature distinguishes central nervous system metastases from primary tumours in non-small-cell lung cancer. *Eur J Cancer*. 2020;132:24–34.
53. Song SG, et al. Comparative analysis of the tumor

- immune-microenvironment of primary and brain metastases of non-small-cell lung cancer reveals organ-specific and EGFR mutation-dependent unique immune landscape. *Cancer Immunol Immunother.* 2021;70(7):2035–2048.
54. Li M, et al. Immune suppressive microenvironment in brain metastatic non-small cell lung cancer: comprehensive immune microenvironment profiling of brain metastases versus paired primary lung tumors (GASTO 1060). *Oncoimmunology.* 2022;11(1):2059874.
 55. Fischer GM, et al. Molecular profiling reveals unique immune and metabolic features of melanoma brain metastases. *Cancer Discov.* 2019;9(5):628–645.
 56. Zacksenhaus E, et al. Mitochondrial OXPHOS induced by RB1 deficiency in breast cancer: implications for anabolic metabolism, stemness, and metastasis. *Trends Cancer.* 2017;3(11):768–779.
 57. Yochum ZA, et al. A first-in-class TWIST1 inhibitor with activity in oncogene-driven lung cancer. *Mol Cancer Res.* 2017;15(12):1764–1776.
 58. Burns TF, et al. Inhibition of TWIST1 leads to activation of oncogene-induced senescence in oncogene-driven non-small cell lung cancer. *Mol Cancer Res.* 2013;11(4):329–338.
 59. Kim SJ, et al. Astrocytes upregulate survival genes in tumor cells and induce protection from chemotherapy. *Neoplasia.* 2011;13(3):286–298.
 60. Jeevan DS, et al. Molecular pathways mediating metastases to the brain via epithelial-to-mesenchymal transition: genes, proteins, and functional analysis. *Anticancer Res.* 2016;36(2):523–532.
 61. Yang Y, et al. ctDNA as a biomarker in phase II study of tepotinib in advanced solid cancers with *MET* exon 14 skipping mutation or amplification (KCSG AL19-17). *J Clin Oncol.* 2024;42(16_suppl):3050.
 62. Kang EJ, et al. A phase II study of tepotinib in patients with advanced solid cancers harboring *MET* exon 14 skipping mutations or amplification (KCSG AL19-17). *ESMO Open.* 2024;9(9):103668.
 63. Priedigkeit N, et al. Intrinsic subtype switching and acquired ERBB2/HER2 amplifications and mutations in breast cancer brain metastases. *JAMA Oncol.* 2017;3(5):666–671.
 64. Di WY, et al. The diagnostic significance of cerebrospinal fluid cytology and circulating tumor DNA in meningeal carcinomatosis. *Front Neurol.* 2023;14:1076310.
 65. Tripathy A, et al. Longitudinal CSF tumor cell enumeration and mutational analysis as a driver for leptomeningeal disease management. *Cancers (Basel).* 2025;17(5):825.
 66. Liu X, et al. Molecular characteristics and prognostic factors of leptomeningeal metastasis in non-small cell lung cancer. *Clin Neurol Neurosurg.* 2023;225:107572.
 67. Zhao W, et al. The potential of radiomics nomogram in non-invasively prediction of epidermal growth factor receptor mutation status and subtypes in lung adenocarcinoma. *Front Oncol.* 2019;9:1485.
 68. Zinn PO, et al. A coclinical radiogenomic validation study: conserved magnetic resonance radiation appearance of perioxin-expressing glioblastoma in patients and xenograft models. *Clin Cancer Res.* 2018;24(24):6288–6299.
 69. Zinn PO, et al. Distinct radiomic phenotypes define glioblastoma TP53-PTEN-EGFR mutational landscape. *Neurosurgery.* 2017;64(suppl_1):203–210.
 70. Park YW, et al. Diffusion tensor and postcontrast T1-weighted imaging radiomics to differentiate the epidermal growth factor receptor mutation status of brain metastases from non-small cell lung cancer. *Neuroradiology.* 2021;63(3):343–352.
 71. Li Y, et al. Differentiating EGFR from ALK mutation status using radiomics signature based on MR sequences of brain metastasis. *Eur J Radiol.* 2022;155:110499.
 72. Zheng L, et al. Radiomic signatures for predicting EGFR mutation status in lung cancer brain metastases. *Front Oncol.* 2022;12:931812.
 73. Lv X, et al. Multisequence MRI-based radiomics signature as potential biomarkers for differentiating KRAS mutations in non-small cell lung cancer with brain metastases. *Eur J Radiol Open.* 2024;12:100548.
 74. Tabnak P, et al. A Bayesian meta-analysis on MRI-based radiomics for predicting EGFR mutation in brain metastasis of lung cancer. *BMC Med Imaging.* 2025;25(1):44.
 75. Xia Y, et al. Targeting HGF/c-MET signaling to regulate the tumor microenvironment: Implications for counteracting tumor immune evasion. *Cell Commun Signal.* 2025;23(1):46.
 76. Benkhoucha M, et al. c-Met⁺ cytotoxic T lymphocytes exhibit enhanced cytotoxicity in mice and humans in vitro tumor models. *Biomedicines.* 2023;11(12):3123.
 77. Glodde N, et al. Reactive neutrophil responses dependent on the receptor tyrosine kinase c-MET limit cancer immunotherapy. *Immunity.* 2017;47(4):789–802.
 78. Peng S, et al. EGFR-TKI resistance promotes immune escape in lung cancer via increased PD-L1 expression. *Mol Cancer.* 2019;18(1):165.
 79. Ahn HK, et al. MET receptor tyrosine kinase regulates the expression of co-stimulatory and co-inhibitory molecules in tumor cells and contributes to PD-L1-mediated suppression of immune cell function. *Int J Mol Sci.* 2019;20(17):4287.
 80. Singhal E, et al. A novel role for Bruton's tyrosine kinase in hepatocyte growth factor-mediated immunoregulation of dendritic cells. *J Biol Chem.* 2011;286(37):32054–32063.
 81. Akli A, et al. Role of the HGF/c-MET pathway in resistance to immune checkpoint inhibitors in advanced non-small cell lung cancer. *Cancer Immunol Immunother.* 2025;74(2):58.
 82. Kubo Y, et al. Serum concentrations of HGF are correlated with response to anti-PD-1 antibody therapy in patients with metastatic melanoma. *J Dermatol Sci.* 2019;93(1):33–40.
 83. Zhang Y, et al. MET amplification attenuates lung tumor response to immunotherapy by inhibiting STING. *Cancer Discov.* 2021;11(11):2726–2737.
 84. Yen BL, et al. Multipotent human mesenchymal stromal cells mediate expansion of myeloid-derived suppressor cells via hepatocyte growth factor/c-met and STAT3. *Stem Cell Reports.* 2013;1(2):139–151.
 85. Yang X, et al. FAP Promotes immunosuppression by cancer-associated fibroblasts in the tumor microenvironment via STAT3-CCL2 signaling. *Cancer Res.* 2016;76(14):4124–4135.
 86. Giannoni P, et al. Chronic lymphocytic leukemia nurse-like cells express hepatocyte growth factor receptor (c-MET) and indoleamine 2,3-dioxygenase and display features of immunosuppressive type 2 skewed macrophages. *Haematologica.* 2014;99(6):1078–1087.
 87. Lee JC, et al. HNC0014, a multi-targeted small-molecule, inhibits head and neck squamous cell carcinoma by suppressing c-Met/STAT3/CD44/PD-L1 oncoimmune signature and eliciting antitumor immune responses. *Cancers (Basel).* 2020;12(12):3759.
 88. Song KY, et al. MET receptor tyrosine kinase inhibition reduces interferon-gamma (IFN- γ)-stimulated PD-L1 expression through the STAT3 pathway in melanoma cells. *Cancers (Basel).* 2023;15(13):3408.
 89. Wakuda K, et al. Efficacy of pembrolizumab in patients with brain metastasis caused by previously untreated non-small cell lung cancer with high tumor PD-L1 expression. *Lung Cancer.* 2021;151:60–68.
 90. Tsuchiya-Kawano Y, et al. Nivolumab plus ipilimumab with chemotherapy for non-small cell lung cancer with untreated brain metastases: a multicenter single-arm phase 2 trial (NIKE, LOGiK 2004). *Eur J Cancer.* 2024;212:115052.
 91. Reck M, et al. Systemic and intracranial outcomes with first-line nivolumab plus ipilimumab in patients with metastatic NSCLC and baseline brain metastases from CheckMate 227 Part 1. *J Thorac Oncol.* 2023;18(8):1055–1069.
 92. Boschert V, et al. The influence of met receptor level on HGF-induced glycolytic reprogramming in head and neck squamous cell carcinoma. *Int J Mol Sci.* 2020;21(2):471.
 93. Yan B, et al. Paracrine HGF/c-MET enhances the stem cell-like potential and glycolysis of pancreatic cancer cells via activation of YAP/HIF-1 α . *Exp Cell Res.* 2018;371(1):63–71.
 94. Natan S, et al. Interplay between HGF/SF-Met-Ras signaling, tumor metabolism and blood flow as a potential target for breast cancer therapy. *Oncoscience.* 2014;1(1):30–38.
 95. Raez LE, et al. A phase I dose-escalation trial of 2-deoxy-D-glucose alone or combined with docetaxel in patients with advanced solid tumors. *Cancer Chemother Pharmacol.* 2013;71(2):523–530.
 96. Redman RA, et al. A phase I, dose-escalation, multi-center study of PFK-158 in patients with advanced solid malignancies explores a first-in-man inhibitor of glycolysis. *J Clin Oncol.* 2015;33(15_suppl):TPS2606.
 97. Pajak B, et al. Synergistic anticancer effect of glycolysis and histone deacetylases inhibitors in a glioblastoma model. *Biomedicines.* 2021;9(12):1749.
 98. Sun J, et al. High levels of ubidecarenone (oxidized CoQ₁₀) delivered using a drug-lipid conjugate nanodispersion (BPM31510) differentially affect redox status and growth in malignant glioma versus non-tumor cells. *Sci Rep.* 2020;10(1):13899.
 99. Gesta S, et al. BPM31510, a clinical stage metabolic modulator demonstrates therapeutic efficacy in an C6 rat glioma model and synergizes with temozolomide. *Cancer Res.* 2017;77(13 suppl):4067.

100. Narain N, et al. Effect of pretreatment, dose and route of administration of BPM31510 (Coenzyme Q10 containing proprietary formulation) alone or in combination with gemcitabine improves survival in pancreatic cancer. *Cancer Res.* 2014;74(19 suppl):4321.
101. Stockdale B, et al. A phase II study of BPM31510 (a lipid nanodispersion of oxidized CoQ10) with vitamin K in combination with standard of care (SOC) RT and TMZ in glioblastoma multiforme (GBM) patients without prior therapy. *Ann Oncol.* 2024;35:S426.
102. Nagpal S, et al. Phase I study of BPM31510 and vitamin K in patients with high grade glioma recurrent after a bevacizumab-containing regimen. *J Clin Oncol.* 2020;38(15_suppl):2543.
103. Kundranda MN, et al. Phase II trial of BPM31510-IV plus gemcitabine in advanced pancreatic ductal adenocarcinomas (PDAC). *J Clin Oncol.* 2020;38(4_suppl):723.
104. Recht L, et al. A phase I study of Bpm31510 plus vitamin K in subjects with high-grade glioma that has recurred on a bevacizumab-containing regimen. *Neuro Oncol.* 2019;21(suppl 8):vi27.
105. Niewiarowska AA, et al. A phase II clinical investigation of BPM31510-IV (ubidecarenone) in patients with advanced pancreatic cancer. *Ann Oncol.* 2018;29(suppl 8):vii270.
106. Narain NR, et al. A phase I molecular adaptive clinical study to evaluate safety and tolerability of BPM31510-IV in advanced solid tumors: final study results. *J Clin Oncol.* 2018;36(15_suppl):2541.
107. Yochum ZA, et al. Targeting the EMT transcription factor TWIST1 overcomes resistance to EGFR inhibitors in EGFR-mutant non-small-cell lung cancer. *Oncogene.* 2019;38(5):656–670.
108. Eckerich C, et al. Hypoxia can induce c-Met expression in glioma cells and enhance SF/HGF-induced cell migration. *Int J Cancer.* 2007;121(2):276–283.
109. Glück AA, et al. Identification of a MET-eIF4G1 translational regulation axis that controls HIF-1 α levels under hypoxia. *Oncogene.* 2018;37(30):4181–4196.
110. Pennacchietti S, et al. Hypoxia promotes invasive growth by transcriptional activation of the met protooncogene. *Cancer Cell.* 2003;3(4):347–361.
111. Chen HH, et al. Hypoxia-inducible factor-1 α correlates with MET and metastasis in node-negative breast cancer. *Breast Cancer Res Treat.* 2007;103(2):167–175.
112. Xia S, et al. Mesothelin promotes brain metastasis of non-small cell lung cancer by activating MET. *J Exp Clin Cancer Res.* 2024;43(1):103.